The following publication Kai Wang, Zhongqing Su, and Shenfang Yuan "Evaluation of crack orientation using fatigue crack-induced contact acoustic nonlinearity", Proc. SPIE 10600, Health Monitoring of Structural and Biological Systems XII, 1060009 (27 March 2018) is available at https://doi.org/10.1117/12.2296475.

Evaluation of crack orientation using fatigue crack-induced contact acoustic nonlinearity

Kai Wang[a], Zhongqing Su[*a,b], Shenfang Yuan[c]
[a]Department of Mechanical Engineering, The Hong Kong Polytechnic University Kowloon, Hong Kong SAR
[b]The Hong Kong Polytechnic University Shenzhen Research Institute, Shenzhen 518057, PR China
[c]State Key Lab of Mechanics and Control of Mechanical Structures, Nanjing University of Aeronautics and Astronautics, Nanjing 210016, P.R. China

ABSTRACT

Based on the two-dimensional (2D)[1] and three-dimensional (3D)[2] analytical models previously developed for interpreting the contact acoustic nonlinearity (CAN) generated due to the modulation from a "breathing" crack in solid media on propagating guided ultrasonic waves (GUWs), this study proposes a new characterization approach, able to orientate a fatigue crack, even when the crack is at its embryo stage. CAN embodied in the scattered Lamb waves and shear horizontal (SH) waves converted from incident GUWs is extracted upon interaction with fatigue cracks, and the unique scattering pattern of CAN is associated with crack slant via the 3D analytical models, whereby the orientation of a fatigue crack can be pinpointed, without making a reference to the baseline signal. Experimental validation of the characterization approach is implemented, in which an undersized fatigue crack is orientated accurately and visualized in the image.

Keywords: contact acoustic nonlinearity; fatigue crack orientation; breathing crack; guided ultrasonic waves

1. INTRODUCTION

Fatigue crack is a prevailing defect in real world engineering structures, which imposes immense threat to the health, safety and integrity of engineering structures. Development and growth of fatigue crack embraces two stages in general cases, *i.e.* the initiation of fatigue crack and crack growth at macro scale, with the former dominating the service life[3]. In the initiation stage, although the fatigue crack growth demonstrates a zigzag-like trend at a micro level, there exists a principal direction in which the crack propagates at macro level. Knowing this principal direction provides the basis for the structural life prediction and structural design/optimization which could enhance the structural integrity and safety[4]. Conventional non-destructive evaluation techniques and structural health monitoring (SHM) techniques, making use of the linear features of the guided ultrasonic waves to detect fatigue damage, have attracted intense research efforts and have been implemented and commercialized in real-world engineering applications. These methods have merits in detecting and characterizing damages with dimensions comparable to the wavelength of probing guided ultrasonic waves (GUWs), nevertheless, in the attempt to evaluate the initiation of a fatigue crack which is always undersized, these methods are confronted with the bottleneck in terms of detectability and sensitivity[5]. Interaction of probing GUWs with damages induces the generation of nonlinear features in the captured wave signals, typified by high-order harmonics, sub-harmonics and shift of resonance frequency, *etc.*, and methods based on these nonlinear features[6-8] have been intensively researched and are demonstrably effective for the improvement of sensitivity of SHM methods.

Most of these nonlinear methods exploit the nonlinear features in GUWs attributed to the material nonlinearity, which is

uniformly distributed in the intact medium and can be intensified by the present damage induced by various sources. In particular, in structures subjected to repeated loading, fatigue damage can be developed at locations undergoing stress concentration due to the geometries and external loading, and in the limited fatigued region such as the vicinity of crack tip, plasticity is introduced, inducing the intensification in material nonlinearity. Yet outside this region, the plasticity induced in the medium is ignorable, and the consequent increase in material nonlinearity is insignificant. It is therefore that when probing GUWs traversing the fatigue damage region, inconspicuously abnormal increase in the nonlinearity of GUWs can be induced by the localized material nonlinearity intensification. On the contrary, compared with the plasticity-driven nonlinearity in GUWs, the contact acoustic nonlinearity induced by the modulation of a "breathing" crack on the propagation of GUWs is remarkable and dominates the nonlinearity in GUWs. Therefore, existing methods addressing material nonlinearity might indicate the presence of fatigue damage qualitatively, but incapable of achieving a quantitative evaluation of the fatigue damage, *e.g.* the orientation and the severity of the fatigue crack. Methods exploiting CAN can potentially fulfill this desire.

The CAN is generated individually and locally at the fatigue crack when probing GUWs traversing and does not rely on the accumulation along the propagation path which entails the satisfaction of the internal resonance requirements, *i.e.* the phase velocity matching and non-zero power flux[9]. It is therefore that different from the limited number of applicable wave mode pairs in existing methods which satisfy the above requirements, waves in low frequency regime can be employed to probe the fatigue crack which are relatively less dispersive and slightly attenuative. As an additional merit, the waves in this range are phase mis-matching and the accumulated nonlinear features in GUWs induced by the material nonlinearity are bounded and oscillating, beneficial for the extraction of CAN. The CAN has attracted intensive research efforts. Wan et al.[10], and Shen and Giurgiutiu[11] investigated the interaction of probing GUWs with a buried micro-crack and a surface-breathing crack in a thin plate in virtue of a finite-element method (FEM), respectively, demonstrating the monotonic increasing of CAN against the length of the micro-crack. Solodov et al.[12] and Richardson[13] explored the generation of high-order harmonics due to the interaction between probing GUWs and a contact crack in one-dimensional scenario, from an analytical perspective. Nevertheless, these studies cannot interpret the generation of CAN when probing GUWs traversing a fatigue crack in a waveguide in three-dimensional scenario accurately, and are not capable of identifying the crack at an initial stage and to further evaluate the crack orientation and severity quantitatively. There exists a lack of know-how about using the CAN to characterize damage.

Motivated by this, in this study we developed a dedicated analytical model which is able to interpret the modulation mechanism of CAN of a "breathing" crack on GUWs and generation of high-order harmonics. In conjunction with the elasto-dynamic method, this model studies the "breathing" crack-induced wave fields and analyses the scattering pattern of the CAN, whereby the orientation of the crack can be evaluated. Validation of the model is to be implemented by comparing the results with those from finite element simulation and experiments. The paper is organized as follows: modulation mechanism of CAN on GUWs propagation are investigated and detailed in Section 2. In this section, the scattering pattern crack-induced CAN which is associated with the crack orientation is developed. Validation of the pattern from finite element simulation and experiment is reported in Section 3. This paper is concluded with Section 4.

2. GENERATION AND SCATTERING PATTERN OF CAN

Consider a three-dimensional plate-like waveguide, in which a through-thickness crack is developed, as schematically shown in Figure 1. Probing GUWs taking the modality of Lamb waves are excited to traverse a crack, and upon the interaction with the crack, the probing GUWs are modulated and scattered, inducing reflection, transmission, diffraction and mode conversions. As commented in section 1, GUWs at low frequency range, as highlighted by a rectangle in Figure 2, are considered in the present study. In this range, the fundamental symmetric (S_0) and anti-symmetric (A_0) Lamb modes co-exist in the waveguide. The S_0 mode features a higher velocity than that of the A_0 mode, beneficial to avoid the contamination from the boundary reflected waves, and is more apt to trigger the "breathing" behavior of the crack. It is therefore that the S_0 mode is selected to interact with the crack and generate the CAN.

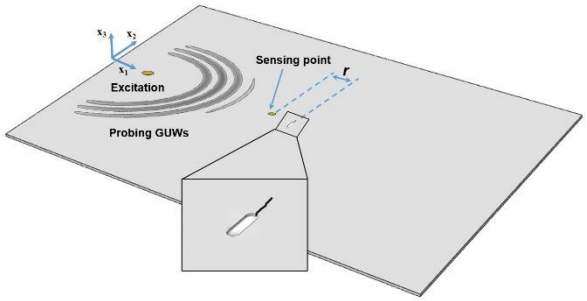

Figure 1. A plate bearing a "breathing" crack

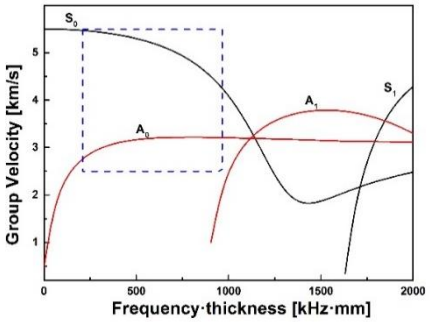

Figure 2. Dispersion curve for an aluminium plate

Although in regions around crack tip the material nonlinearity is intensified by the crack-induced plasticity, the corresponding abnormal increase of high-order harmonics in GUWs are negligible compared with the counterpart caused by "breathing" behaviour of the crack, because waves at the incident frequency (300 kHz) does not satisfy the internal resonance requirements, and thus the amplitude of second harmonic in GUW is bounded and oscillating[14]. It is therefore that the nonlinear features related with the plasticity is not taken into account in the present study and only the CAN-induced nonlinearity is investigated.

When traversing the fatigue crack, the probing GUWs are modulated by the "breathing" behaviour of the crack and contact acoustic nonlinearity is induced and embodied in the waves scattered by the crack. The interaction between the GUWs and

the crack embraces two states: 1) crack opening during the tensile phase of probing GUW, leading to wave scattering and mode conversion; and 2) crack closing during the compressional phase of probing GUW and the GUW traverses the crack continuously without being distorted. Both these states jointly compose the "breathing" behaviour, and therefore a "breathing" crack can be deemed as a second wave source in the waveguide to introduce an additional wave field that modulates the original wave field, and therefore this source is called "*crack-induced second source*" (CISS hereinafter) in what follows.

During the crack opening, the crack surfaces are stress-free and the CISS on the crack surfaces can be depicted using the equilibrant forces for the stress field induced by the probing GUW on the crack surfaces. Note that the fatigue crack studied in this paper is in its initiation stage, the scale of the crack (at a micro level) is such insignificant compared with the distance between the receivers and the crack that the CISS at the crack is equivalent to a concentrated force whose magnitude can be calibrated using the integration of the CISS over the crack surface, as

$$\overrightarrow{CISS}^{open} = \int_{Crack\ Surface} -\tilde{\sigma}^{inc} \cdot \vec{x}_1 ds. \tag{1}$$

In the above, $\tilde{\sigma}^{inc}$ is the stress tensor of the incident probing GUW and $\vec{x}_1$ signifies the direction vector. $\overrightarrow{CISS}^{open}$ denotes the crack-induced second source when the crack opens.

The CISS is present during crack opening and absent otherwise. Considering the ignorable influence of the crack initiation on the wave fields in the waveguide, the moment when the traversing waves turn from compression into the tension and the moment when traversing waves turn from tension into compression are adopted as the moment for crack opening (denoted as t_{open}) and closing (denoted as t_{close}), respectively. Accordingly, the duration of the crack opening, in which the CISS is generated, is the half period in a cycle of the probing GUW, as shown in Figure 3(a). To reflect the above periodical characteristic of the "breathing" behavior, an indicator function $f(t)$, is introduced to modulate $\overrightarrow{CISS}^{open}$

$$\overrightarrow{CISS}^{bre} = \overrightarrow{CISS}^{open} \cdot \mathrm{e}^{i\omega_0 t} \cdot f(t), \tag{2}$$

where

$$f(t) = \begin{cases} 1, & t_{open} < t < t_{close} \\ 0, & t_{close} < t < t_{open} + T, \end{cases} \tag{3}$$
$$t_{close} = t_{open} + T/2.$$

In Eq. (2), $\overrightarrow{CISS}^{bre}$ is the modulated CISS attributed to the "breathing" behavior. ω_0 is the angular frequency of the probing GUW. T is the duration of a cycle of the probing GUW. With Eqs. (2)-(3), the spectrum of $\overrightarrow{CISS}^{bre}$ can be obtained, from which each high-order component can be ascertained, as shown in Figure 3(b).

With the obtained magnitude of double excitation frequency ($2\omega_0$) components, $\overrightarrow{CISS}^{bre}$ at $2\omega_0$ can be depicted as

$$\overrightarrow{CISS}^{bre-2\omega_0} = A_{2\omega_0} \cdot \overrightarrow{CISS}^{open} \cdot e^{i2\omega_0 t}. \quad (4)$$

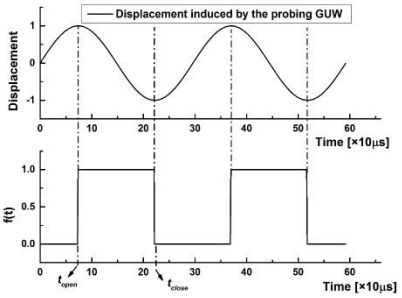

(a)

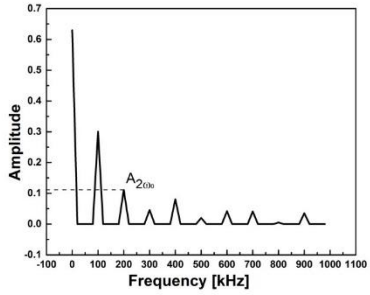

(b)

Figure 3. (a) Indicator function; (b) spectrum of the CISS

With the Eq. (4), the $\overrightarrow{CISS}^{bre-2\omega_0}$ can be ascertained in an explicit modality. The orientation of the crack which is to be evaluated, imposes significant influence on the wave scattering and generation of nonlinearity in the probing GUWs. To scrutinize the orientation-induced influence, consider a fatigue crack which orientates not tangentially to the wave front of probing GUWs, the waves are captured at different sensing points, as schematically shown in Figure 4.

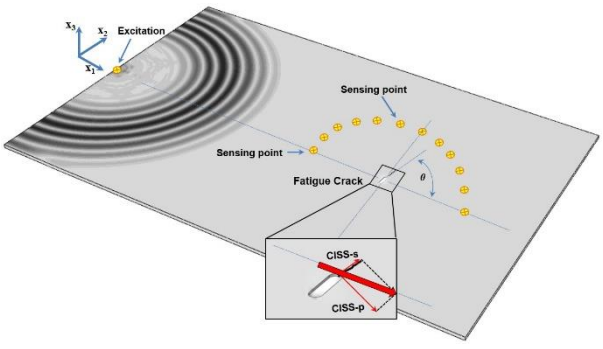

Figure 4. Probing GUWs interact with a crack orientates not tangentially to the wavefront

In this scenario, the $\overrightarrow{CISS}^{bre-2\omega_0}$ on the crack surfaces can be decomposed into two components: the $\overrightarrow{CISS}_P$ which is perpendicular to the crack surfaces and the $\overrightarrow{CISS}_S$ which is parallel to crack surface. Note that the *CISS* on a crack surface points at the opposite direction to the *CISS* on the other crack surface. The waves generated by the $\overrightarrow{CISS}_S$ on both surfaces, including symmetric Lamb waves and SH waves, principally propagate along the crack orientation, and have the identical amplitude yet opposite phase, thus cancelling each other out. On the contrary, the $\overrightarrow{CISS}_P$ induce waves in the same manner as in a normal incidence case and the symmetric Lamb waves generated by the $\overrightarrow{CISS}_P$ on each crack surface propagate independently, imposing no influence on each other, and thus can be detected. Accompanying the scattering of Lamb waves, in the vicinity of the crack tip, the stress concentration at the crack tip leads to the particulate displacement along the crack orientation and the consequent generation of SH waves which principally propagate perpendicularly to the crack orientation. It is therefore that the generation of CAN is attributed to the $\overrightarrow{CISS}_P$ which features time-dependent traits.

Note that the generation of Lamb waves and converted SH waves are principally attributed to the in-plane component $CISS_P^{in}$ of $\overrightarrow{CISS}_P$, thus only $CISS_P^{in}$ is considered in what follows. Based on the elasto-dynamic method[15], the displacement of the Lamb waves and SH waves in the direction of $\vec{x}_1$ induced by the $CISS_P^{in}$ can be predicted, as

$$
\begin{aligned}
&{}_{2\omega_0}u_{x_1}^{S_0} = A^{S_0}U^{S_0}(x_3)\left[H_0^2\left(k_{S_0}r\right)-\frac{1}{k_{S_0}r}H_1^2\left(k_{S_0}r\right)\right]\cos\left(\theta_1-\left(\frac{\pi}{2}+\theta\right)\right)\cos(\theta_1),\\
&A^{S_0} = \frac{k_{S_0}}{4i}\frac{CISS_p^{in}U^{S_0}(x_3)}{I_{S_0S_0}},\\
&{}_{2\omega_0}u_{x_1}^{SH_0} = B^{SH_0}\frac{1}{k_{SH_0}r}H_1^2\left(k_{SH_0}r\right)\cos\left(\theta_1-\left(\frac{\pi}{2}+\theta\right)\right)\sin(\theta_1),\ B^{SH_0}=\frac{1}{4i}\frac{1}{2\mu h}f\left(CISS_p^{in}\right).
\end{aligned}
\tag{5}
$$

In the above, ${}_{2\omega_0}u_{x_1}^{S_0}$ and ${}_{2\omega_0}u_{x_1}^{SH_0}$ are the displacement fields of the propagating S_0 and SH_0 modes at $2\omega_0$, respectively. k_{S_0} and k_{SH_0} are the wavenumber of the propagating S_0 mode and SH_0 mode at $2\omega_0$, respectively. i is the imaginary unit. θ_1 is the angle between the path linking the crack and sensing point and the $\vec{x}_1$ direction. r is the distance from the crack to the sensing point as shown in Figure 1. $U^{S_0}(x_3)$ denotes the shape function of the in-plane displacement of S_0 mode at $2\omega_0$. H is the Hankel function. h is the half thickness of the medium. μ is the shear modulus. $I_{S_0S_0}$ is the power carried by the S_0 mode. f, as a function of $CISS_p^{in}$, is the equivalent force which induces the generation of converted SH_0 mode. For the purpose of orientating the crack, the amplitude of f is not prerequisite and thus not analyzed in this study. With Eq. (5), the wave scattering pattern which is correlated with the crack orientation can be depicted analytically, and inversely, using the nonlinear features in GUW signals captured from different sensing points, this pattern can be exploited to calibrate the orientation of the crack. Note that the ${}_{2\omega_0}u_{x_1}^{S_0}$ and ${}_{2\omega_0}u_{x_1}^{SH_0}$ are also linked with the crack length, and therefore their amplitudes can also be used to estimate crack parameters and to indicate the severity of the crack in a quantitative manner.

3. PROOF-OF-CONCEPT VALIDATION

For validation of the proposed model in 3D scenario, an aluminium plate, measuring 2mm in thickness, 500mm in length and 600mm in width, was meshed and analysed with ABAQUS®/EXPLICIT. The properties of the aluminium plate are listed in Table 1.

Table 1. Material and physical properties of the aluminum used in FE validation

Density (Kg/m^3)	E (GPa)	υ	c_L (m/s)	c_T (m/s)
2660	71.8	0.33	6324	3185

The slant angle between the dominant crack orientation and propagation direction ($\vec{x}_1$) of the probing GUW was set to be 75°. A five-cycle Hanning-windowed sinusoidal tone burst in the form of symmetric propagating mode (S0) were produced by applying a pair of point forces at two points on the upper and lower surface, respectively, which were symmetric about the middle plane of the waveguide at incident frequency (300kHz). To model the "breathing" crack in the plate, a seam crack with stress-free surfaces was define, and a contact-pair interaction between the crack surfaces was applied as well.

The time-series of in-plane displacement in the $\vec{x}_1$ direction were extracted from twelve FE points (serving as sensing points) which were located along the periphery of a semi-circle centred at the crack (30 mm from the crack center) and 15° apart between any two adjacent points, as shown in Figure 4. Note that the amplitude of second harmonics induced by the damage in the structures was lower than probing waves by orders, and thus making the extracted second harmonics prone to the influence of fundamental waves, as the bandwidth of exciting tone burst was not sufficiently narrow. To tackle this disadvantage, a pulse-inversion technique was deployed, in which the point force used to excite the incident waves in a simulation being the inversion of that applied in another simulation. In virtue of adding up the recorded signals in both simulations, the damage-induced second harmonic can be intensified while the fundamental waves were reduced remarkably, beneficial for extracting second harmonics precisely, as shown in Figure5.

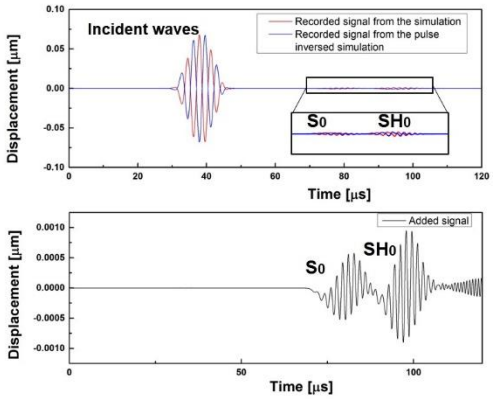

Figure 5. The recorded signal in simulations and the added signal using pulse-inversion technique

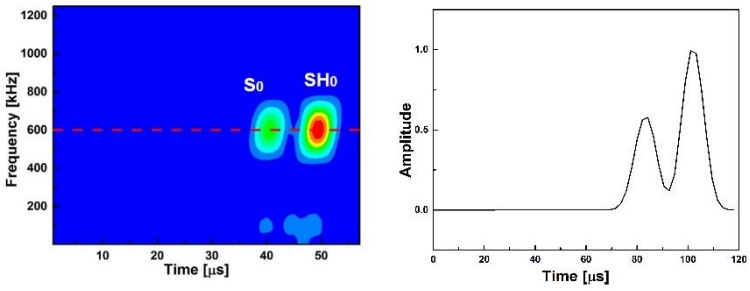

(a) (b)

Figure 6. (a) Spectrum of the added wave signals in Figure 5; (b) spectrum of the added signals at $2\omega_0$

After processing the captured wave signals using the short time Fourier transform (STFT) technique, the spectra of the acquired wave signals can be obtained as shown in Figure 6, from which the amplitude of crack-induced Lamb waves (${}_{2\omega_0}u_{x_1}^{S_0}$) and SH waves (${}_{2\omega_0}u_{x_1}^{SH_0}$) at $2\omega_0$ can be obtained. The correlation of the amplitude of each crack-induced waves against the sensing position is shown in Figure 7. Comparison between the results from simulation and the prediction from the analysis in Section 2 exhibits good coincidence.

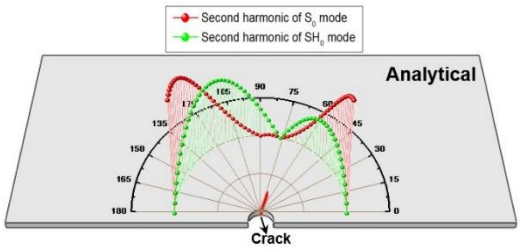

(a)

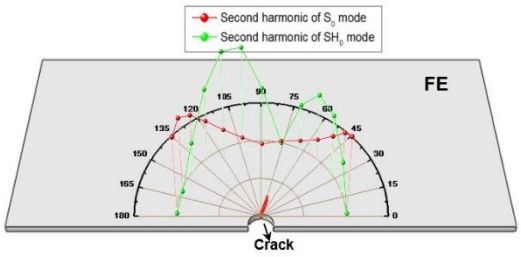

(b)

Figure 7. Wave scattering patterns (linked to the crack orientation) obtained from (a) analytical, and (b) FE methods

In the experiment, an aluminium plate, measuring 500mm in length and 300mm in width was examined, whose properties were identical with those listed in Table 1. To initiate the fatigue crack, a through-thickness slot was treated at the centre of the plate, which was small enough (measures 5mm in length) to warrant that the influence it imposes on the propagation of probing GUWs was ignorable. A through-thickness fatigue crack was introduced to the specimen at the tip of the slot, by applying 120000 cycles of a cyclic tensile loading (5-26 kN; ration is 0.19) at a 10 Hz cycle frequency using a fatigue

test machine (GP-SDF2000). A five-cycle Hanning-windowed sinusoidal tone burst at 300 kHz was excited using a computer controlled ultrasonic system (RITEC® SNAP system), which was processed using a filter to filter out the second harmonics in the tone burst before being fed into a transducer(Olympus V1548) mounted on the surface of the plate. The in-plane displacements of twelve sensing points in the $\vec{x}_1$ direction, which were located at the periphery centred at the crack, were acquired using a laser vibrometer system at a sampling rate of 50 MHz, as shown in Figure 8. The angle in between the adjacent points was 15°, which was consistent with that in the simulation.

The STFT-based signal processing was employed again to extract the second harmonics from the captured wave signals, and knowing the time of flight of each wave packet and locations of sensing points, the wave mode of each wave packet can be determined according to their velocity. On this basis the amplitude of each wave mode (S_0 and SH_0) induced by the "breathing" behaviour can be ascertained, with which the scattering pattern of the scattered S_0 mode and converted SH_0 mode can be obtained. Figure 8 displays the scattering pattern in a polar coordinate system, to observe that the amplitudes of the crack-induced S_0 and SH_0 modes reach the minimum in the direction of the crack orientation, as the ${}_{2\omega_0}u_{x_1}^{S_0}$ and ${}_{2\omega_0}u_{x_1}^{SH_0}$ is zero in this direction. Compared with the results from the theoretical analysis and simulations, good consistency can be observed in between. Inversely, the orientation of crack, which is at its embryo stage and thus induces indiscernible linear features of GUWs, can be evaluated using the scattering pattern of the crack-induced S_0 mode or SH_0 mode at $2\omega_0$. In addition, knowing the time of flight of each wave mode and the locations of sensing points and excitation source, the location of the crack can be pinpointed using existing methods[16]. It is worth noting that using this method, the measurement of the wave signals are conducted in the current status, and therefore the identification of CAN embodied in the scattered Lamb waves and converted SH waves translate directly into the diagnosis of a fatigue crack without entailing a benchmarking process against the baseline from the intact specimen.

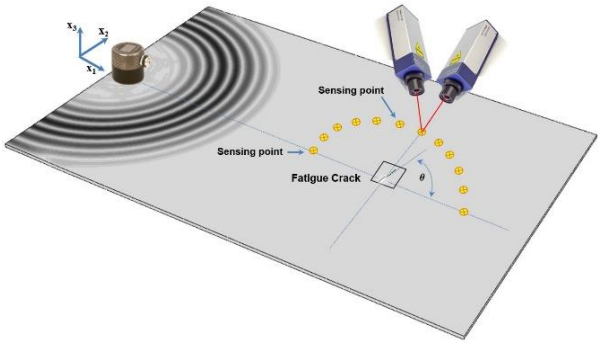

(a)

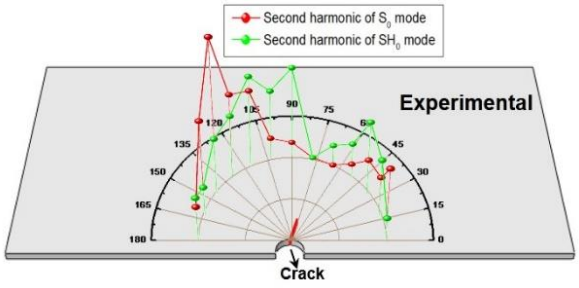

(b)

Figure 8. (a) Experiment set-up; (b) the scattering patterns of crack-induced S0 and SH0 wave modes

4. DISCUSSIONS AND CONCLUDING REMARKS

In this paper, an analytical model is presented to interpret the modulation mechanism of a “breathing” crack on probing waves and the generation of crack-induced second harmonic. In this model, the CAN induced by the “breathing” crack is well interpreted in a 3D scenario by analyzing the “breathing” behavior of a crack and exploiting the elasto-dynamic method. The model investigates the CAN embodied in the scattered Lamb waves and shear horizontal (SH) waves converted from incident GUWs , and the unique scattering pattern of CAN is associated with crack slant via the 3D analytical models, whereby the orientation of fatigue crack can be evaluated in a quantitative manner, even when the crack is at its embryo stage. The proposed method is validated by finite element simulation and experiment. The comparison shows that based on the results obtained using the proposed method, by measuring the crack-induced nonlinear features in GUWs, it is possible to evaluate the orientation of the fatigue crack in a quantitative manner.

ACKNOWLEDGMENTS

This project is supported by National Natural Science Foundation of China (Key Project No. 51635008). This study is also supported by the Hong Kong Research Grants Council via General Research Funds (GRF Nos. 15212417 and 15201416).

REFERENCES

[1] K. Wang and Z. Su, "Analytical modeling of contact acoustic nonlinearity of guided waves and its application to evaluating severity of fatigue damage", SPIE Smart Structures and Materials+ Nondestructive Evaluation and Health Monitoring,98050L-98050L-13 (2016).

[2] K. Wang, Z. Su, and S. Yuan, "A three-dimensional analytical model for interpreting contact acoustic nonlinearity generated by a" breathing" crack", Health Monitoring of Structural and Biological Systems 2017,101701X (2017).

[3] G. Fajdiga and M. Sraml, "Fatigue crack initiation and propagation under cyclic contact loading", Eng. Fract. Mech., 76, 1320-1335 (2009).

[4] J. W. Ringsberg, "Life prediction of rolling contact fatigue crack initiation", International Journal of fatigue, 23, 575-586 (2001).

[5] Z. Su, C. Zhou, M. Hong, L. Cheng, Q. Wang, and X. Qing, "Acousto-ultrasonics-based fatigue damage characterization: Linear versus nonlinear signal features", Mech. Syst. Signal Process, 45, 225-239 (2014).

[6] C. Pruell, J.-Y. Kim, J. Qu, and L. J. Jacobs, "Evaluation of plasticity driven material damage using Lamb waves", Appl. Phys. Lett., 91, 231911 (2007).

[7] J. Potter, A. Croxford, and P. Wilcox, "Nonlinear ultrasonic phased array imaging", Phys. Rev. Lett., 113, 144301 (2014).

[8] J. Pei and M. Deng, "Assessment of fatigue damage in solid plates using ultrasonic lamb wave spectra", Ultrasonics Symposium, 2008. IUS 2008. IEEE,1869-1872 (2008).

[9] W. De Lima and M. Hamilton, "Finite-amplitude waves in isotropic elastic plates", J. Sound Vib., 265, 819-839

(2003).
[10] X. Wan, Q. Zhang, G. Xu, and P. W. Tse, "Numerical simulation of nonlinear lamb waves used in a thin plate for detecting buried micro-cracks", Sensors, 14, 8528-8546 (2014).
[11] Y. Shen and V. Giurgiutiu, "Predictive simulation of nonlinear ultrasonics", Proc. SPIE,83482E (2012).
[12] I. Y. Solodov, "Ultrasonics of non-linear contacts: propagation, reflection and NDE-applications", Ultrasonics, 36, 383-390 (1998).
[13] J. M. Richardson, "Harmonic generation at an unbonded interface—I. Planar interface between semi-infinite elastic media", International Journal of Engineering Science, 17, 73-85 (1979).
[14] P. Zuo, Y. Zhou, and Z. Fan, "Numerical and experimental investigation of nonlinear ultrasonic Lamb waves at low frequency", Appl. Phys. Lett., 109, 021902 (2016).
[15] J. Achenbach and Y. Xu, "Wave motion in an isotropic elastic layer generated by a time-harmonic point load of arbitrary direction", J. Acous. Soc. Am., 106, 83-90 (1999).
[16] M. Hong, Z. Su, Y. Lu, H. Sohn, and X. Qing, "Locating fatigue damage using temporal signal features of nonlinear Lamb waves", Mech. Syst. Signal Process, 60, 182-197 (2015).